Title

Subseasonal Warming of Surface Soil Enhances Precipitation Over the Eastern Tibetan Plateau in Early Summer

Authors

Qi, Xin
Yang, Jing
Xue, Yongkang
et al.

Peer reviewed

JGR Atmospheres

Key Points:

- Surface soil temperature over the eastern Tibetan Plateau (ETP) features subseasonal variations with a quasi-biweekly period in early summer
- The warming surface soil over the ETP could enhance the subseasonal precipitation through altering the lower-level convective instability
- WRF experiments confirm that ETP soil thermal effect on precipitation is much more crucial than soil moisture in the subseasonal time scale

Subseasonal Warming of Surface Soil Enhances Precipitation Over the Eastern Tibetan Plateau in Early Summer

Xin Qi[1,2] [ID], Jing Yang[1] [ID], Yongkang Xue[3] [ID], Qing Bao[4] [ID], Guoxiong Wu[4], and Duoying Ji[5] [ID]

[1]Key Laboratory of Environmental Change and Natural Disaster, Ministry of Education, Faculty of Geographical Science, Beijing Normal University, Beijing, China, [2]Frontiers Science Center for Deep Ocean Multispheres and Earth System (FDOMES), Ocean University of China, Qingdao, China, [3]Department of Geography, University of California Los Angeles, Los Angeles, CA, USA, [4]State Key Laboratory of Numerical Modeling for Atmospheric Sciences and Geophysical Fluid Dynamics, Institute of Atmospheric Physics, Chinese Academy of Sciences, Beijing, China, [5]College of Global Change and Earth System Science, Beijing Normal University, Beijing, China

Abstract The precipitation over the eastern Tibetan Plateau (ETP, here defined as 29°–38°N, 91°–103°E) usually exhibits significant subseasonal variation during boreal summer. As the hot spot of land-air interaction, the influences of ETP surface soil temperature (T_{soil}) on the local precipitation through subseasonal land-air interaction are still unclear but urgently needed for improving subseasonal prediction. Based on station and reanalysis datasets of 1979–2018, this study identifies the evident quasi-biweekly (QBW) (9–30 days) periodic signal of ETP surface T_{soil} variation during the early summer (May–June), which results from the anomalies of southeastward propagating mid-latitude QBW waves in the mid-to-upper troposphere. The observational results further show that the maximum positive anomaly of precipitation over the ETP lags the warmest surface T_{soil} by one phase at the QBW timescale, indicating that the warming surface T_{soil} could enhance the subseasonal precipitation. The numerical experiments using the WRF model further demonstrate the effect of warming surface T_{soil} on enhancing the local cyclonic and precipitation anomaly through increasing upward sensible heat flux, the ascending motion, and water vapor convergence at the QBW timescale. In contrast, the effect of soil moisture over the ETP is much weaker than T_{soil} at the subseasonal timescale. This study confirms the importance of surface T_{soil} over the ETP in regulating the precipitation intensity, which suggests better simulating the land thermal feedback is crucial for improving the subseasonal prediction.

1. Introduction

The Tibetan Plateau (TP) is located in the subtropics of eastern Eurasia, and its climate is under the combined influences of the East Asian, South Asian monsoons (Tao & Ding, 1981; Webster et al., 1998) and of the mid-latitude westerlies (Schiemann et al., 2008). In boreal summer, the atmospheric circulation over the TP features evident subseasonal signals with a significant quasi-biweekly (QBW) periodicity, which strongly modulates the initiation and development of extreme meteorological events in both local and downstream regions (e.g., Duan et al., 2012; Dugam et al., 2009; Wang et al., 2009). The skillful prediction in amplitude and duration of QBW atmospheric anomalies over the TP is crucial for improving local and surrounding subseasonal prediction, but it is still challenging scientifically.

As the hot spot of land-air interaction (Koster et al., 2004; Ma et al., 2010), the TP land has been found to evidently influence the atmosphere through modulating the energy and water budgets in different timescales (e.g., Liu et al., 2020; Wei & Dirmeyer, 2010; Ye, 1981). Most previous studies concentrate on diurnal (e.g., Xu et al., 2002), interannual (e.g., Ullah et al., 2021) and decadal timescales (Zhang et al., 2018), but few studies paid attention to the TP land effect on the atmospheric circulation and precipitation anomaly at the subseasonal timescale.

Some recent studies have underlined the importance of the subseasonal land-air interaction over the TP from the perspective of soil moisture and snow cover. For instance, Wan et al. (2017) pointed out that the drier soil over the TP can increase surface sensible heat flux in summer and enhance an anti-cyclonic anomaly over the Yangtze Basin, thus blocking the northward subseasonal migration of precipitation. Li et al. (2018) reported the evident subseasonal lag relationship between snow cover over the TP and East Asian atmospheric circulation during wintertime. However, the land surface soil temperature (T_{soil}) on subseasonal precipitation over the TP has not been clarified in boreal summer.

The T_{soil} is a primary indicator of land thermal feature and the crucial forcing in coupled climate models (Delworth & Manabe, 1988; Seneviratne et al., 2006; Yeh et al., 1984), which plays an important role in land-air interactions (Yeh et al., 1984) and has wide applications to agricultural production (Deardorff, 1978; Mihalakakou, 2002). For one thing, the T_{soil} has its climate memory ranging from weeks to season, which has been recognized as an important predictability source for subseasonal prediction (e.g., Amenu et al., 2005; Dirmeyer et al., 2018; Mariotti et al., 2018; Yang & Zhang, 2016). The T_{soil} memory over the TP in different land models calculated by Qiu et al. (2021) shows that the averaged lengths of T_{soil} memory at 0.05 m depth fall at the subseasonal range (15.8~54 days), which suggests that T_{soil} potentially influences subseasonal prediction over TP. For another thing, the initialization of T_{soil} has been found to have a significant impact on medium-range prediction (e.g., Guo et al., 2002; Qian & Shen, 1990). Particularly, a recent research project named *Impact of Initialized Land Surface Temperature and Snowpack on Subseasonal to Seasonal Prediction (LS4P)* has reported that the T_{soil} anomaly over the TP in May can evidently affect the lead-1 month prediction of the downstream precipitation based on multi-model experiments (Xue et al., 2018, 2021, 2022). In spite of the strong implications from these pioneer numerical studies, the linkage between the surface T_{soil} and the atmospheric circulation/precipitation and associated physical mechanism at subseasonal timescale has not been well recognized over some core regions of TP.

To explore the influence of surface T_{soil} over the TP on subseasonal prediction, it should first verify the linkage between the surface T_{soil} and atmospheric circulation/precipitation over the TP at the subseasonal timescale. Based on the long-record station and reanalysis datasets, this study aims to investigate the subseasonal features of surface T_{soil} in the plateau region during summer and clarify the T_{soil} effect on the subseasonal precipitation through composite analysis and case modeling experiments. The rest of the article is organized as follows. Section 2 describes the datasets, methodology, and regional model. Section 3 addresses the dominant subseasonal variability of surface T_{soil} over the core region of TP. The influence of the subseasonal atmospheric circulation on surface T_{soil} is presented in Section 4. The numerical results about the land feedback on the atmosphere are comprehensively addressed in Section 5. Finally, the discussion and conclusion are provided in Section 6.

2. Data, Methods, and Model Description

2.1. Data

The daily-mean T_{soil} for the period of 1979–2018 was extracted from the ERA-Interim reanalysis produced by the European Center for Medium Range Weather Forecasts, which has a 0.75° horizontal resolution and four layers in the vertical direction with a top-down thickness of 0.07, 0.21, 0.72, and 1.89 m, respectively (Dee et al., 2011; Simmons et al., 2007). The uppermost T_{soil} is adopted for calculating the surface T_{soil} in this study. The ERA-Interim product is commonly used in TP research and the related regional numerical simulation as a driving dataset (e.g., Gao et al., 2015; Maussion et al., 2014; Ullah et al., 2018). Some previous studies also have demonstrated ERA-interim T_{soil} is reliable in describing the subseasonal variation over the TP region (e.g., Su et al., 2011; Yang et al., 2020). To ensure the robustness of our results, the observational station dataset of T_{soil} over the TP was also retrieved from the National Tibetan Plateau/Third Pole Environment Data Center (Su et al., 2011) to make a comparison, which supports the major results both in the total field and QBW component.

Observational precipitation data from rain gauge stations without missing records over the TP was derived from the China Meteorological Administration (http://data.cma.cn). The geographical locations of the above station are shown in Figure 1a. In addition, the daily atmospheric circulation fields including air temperature, surface pressure, horizontal winds, specific humidity, vertical velocity, and geopotential height were retrieved from the ERA-Interim reanalysis product with a 1.5° horizontal resolution and 37 pressure levels in the vertical coordinate.

2.2. Methods

To identify the specific periodicity of surface T_{soil}, the subseasonal component was first extracted from the raw daily data through removing the climatological mean (defined over 1981–2010) and synoptic fluctuations using a 5-day running mean successively (Qi et al., 2019; Yang et al., 2010). Then power spectrum analysis with a tapered window (Bingham et al., 1967; Gilman et al., 1963) was performed on the time series of subseasonal components in the target period each year. Finally, according to the results of the power spectrum, the band filtering technique using the fast Fourier transform, which has been broadly used at the subseasonal time scale in previous studies (e.g., Bloomfield, 2000; Gao et al., 2018; Hu et al., 2016; Wang & Duan, 2015), was applied
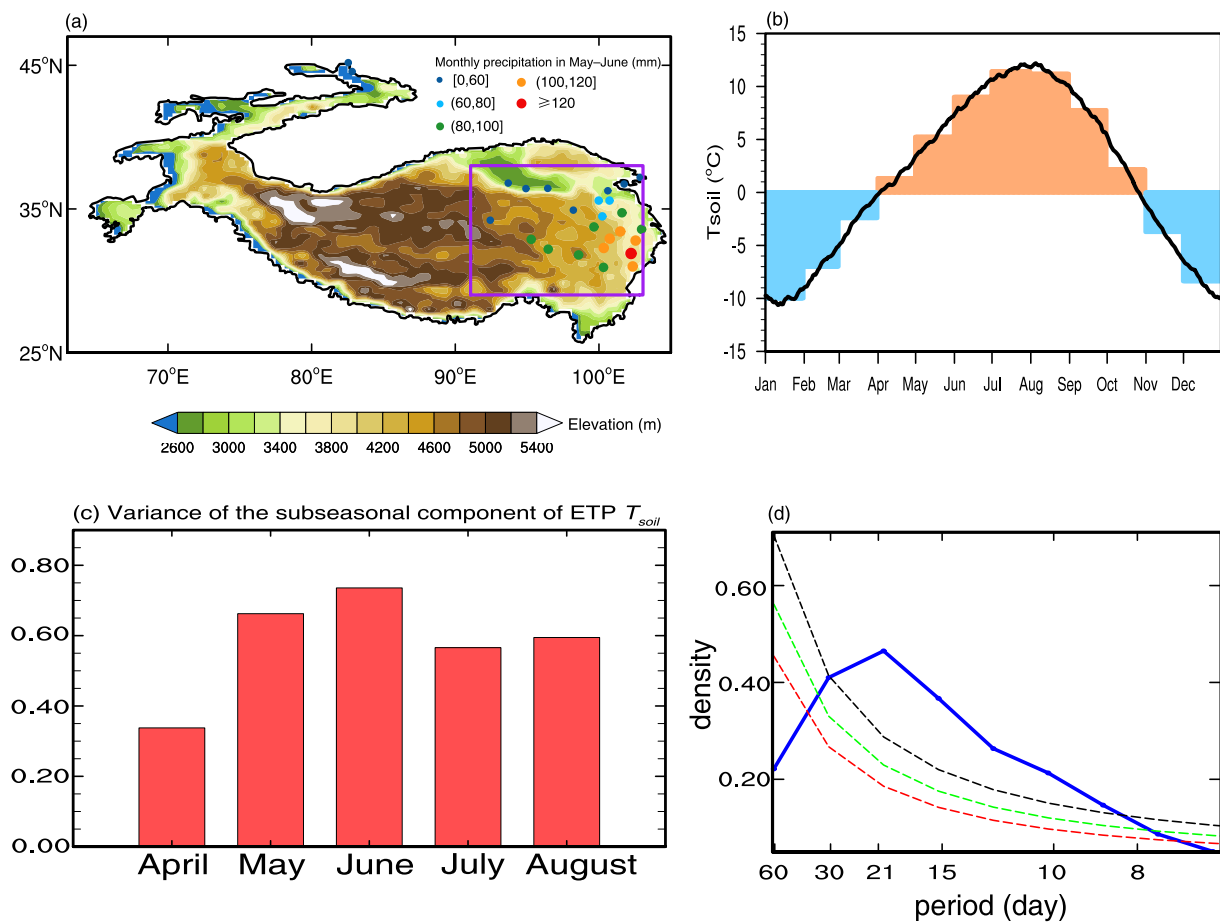
Figure 1. (a) Elevation over the Tibetan Plateau (shadings, m). The dots represent the location of the CMA rain gauge stations and the color of the dots denotes the climatological monthly precipitation (mm) in early summer (May–June). The purple box denotes the eastern Tibetan Plateau (ETP) region. (b) Time series of climatological daily (line) and monthly mean (bars) surface soil temperature (T_{soil}) (°C) averaged over the ETP. (c) The variance of the subseasonal component of surface T_{soil} averaged over the ETP in boreal summer. (d) The 40-year averaged power spectrum of the subseasonal component of daily surface T_{soil} in May and June over the ETP (blue line), compared with Markov red noise spectra (dashed red lines), a priori 99% confidence bound (dashed green lines) and a posterior 99% confidence level (dashed black lines).

to derive the dominant subseasonal signals. Meanwhile, the Lanczos and Butterworth bandpass filters were also applied to extract the subseasonal component to ensure robustness. In reality, the major findings of this work are not sensitive to different filtering methods.

Phase compositing technique (Fujinami & Yasunari, 2004; Gao et al., 2018; Yang et al., 2014) was employed here for describing the common feature of spatial-temporal evolution among selected subseasonal cycles for meteorological variables. This composite analysis is made based on phases. Each subseasonal (band-filtered component) cycle is defined to have eight phases. As shown in Figure S1a in Supporting Information S1, phases 1 and 5 are the dates with the coldest anomaly (the valley) phase and the warmest anomaly (the peak) phase, respectively. Phase 3 and 7 are the dates with zero anomalies. Phases 2 and 8 (4 and 6) are the transitional phases and roughly the middle dates between the minimum (maximum) and zero anomalies. After that, the typical cycles whose peak and valley values exceed ±0.8 times the standard deviation of the subseasonal component were selected as significant events. Thus, the subseasonal structure and propagation are examined based on its life cycle. The *student's-t* test was performed to assess the statistical significance of composite results. To ensure a strict confidence level for statistical test, the effective degree of freedom is estimated according to Pyper and Peterman (1998), the formulation of N_{eff} given by $N_{eff} \approx \frac{N}{1+2\sum_{k=1}^{N} \frac{N-k}{N} r_1(k) r_2(k)}$, where N is 2,440 and $r_1(k)$ and $r_2(k)$ are the lag k-day autocorrelation coefficient of surface T_{soil} and precipitation, respectively.

2.3. Model and Experimental Design

The Advanced Research WRF model (version 4.2), a regional and non-hydrostatic atmospheric simulation system with sigma terrain-following coordinates (Skamarock et al., 2008), was used to investigate the possible feedback of the T_{soil} to the atmosphere. The following physical parameterization schemes were set in the experiments to achieve the best performance: the WRF single moment six class microphysics scheme (Hong & Lim, 2006), the Yonsei University scheme for the planetary boundary layer (Hong et al., 2006), the multi-scale Kain–Fritsch scheme for cumulus parameterization (Glotfelty et al., 2019; Zheng et al., 2016), the RRTMG (rapid radiative transfer model for general circulation models) shortwave and longwave schemes (Iacono et al., 2008), the revised MM5 scheme for surface layer (Jimenez et al., 2012), and the unified Noah land surface model (Tewari et al., 2004). All schemes were taken with default settings and no further tuning are made.

The initial and lateral boundary forcing were taken from ERA-Interim reanalysis at 6-hr intervals and 26 vertical pressure levels from the surface to 10 hPa. As the input of the land model component, the geographical surface data included 21-class MODIS land use data and soil type data from the Food and Agriculture Organization of the United Nations and 30 arcsec terrain elevation data from the U.S. Geological Survey and the National Geospatial-Intelligence Agency. In order to identify the feedback of surface T_{soil} to the atmospheric anomalies, we conducted three ensemble experiments with the same model configuration based on a typical subseasonal event in the early summer of 2018, which will be presented in further detail in Section 5.

3. Subseasonal Variation of Surface T_{soil} Over the Eastern TP

3.1. QBW as the Dominant Subseasonal Periodicity of Surface T_{soil} Over the Eastern TP

Rainy days over the TP usually occur in the boreal summer owing to the TP thermal effect and monsoon flow (Hu et al., 2016; Zhang et al., 2014), and the precipitation predominantly falls over the eastern region of TP (Fu et al., 2020; Maussion et al., 2014). Accompanied by the anomalous cyclonic circulation and convection, the precipitation over the eastern TP (ETP) also features significant QBW variation (e.g., Feng & Zhou, 2012; Fujinami & Yasunari, 2009; Liu et al., 2007; Yang et al., 2017). Since the ETP is the core region of subseasonal rainfall activities in boreal summer and the spatial distribution of the anomalous surface T_{soil} is not uniform over the entire TP domain, we concentrate on the surface T_{soil} over the ETP (here defined as 29°–38°N, 91°–103°E), rather than over the entire domain of TP in this study.

Seasonally frozen surface soil is widely distributed in the alpine region of ETP (Luo et al., 2020; Yang & Wang, 2019) that thaws in summer and refreezes in winter. When this layer's depth increase, the frozen soil freezes deeper in winter, which is different from the active layer underlain by permafrost. When the active layer increases the permafrost thaws deeper (Li et al., 2021). In climatology, the soil over the ETP enters the freeze-thaw period starting from April with the monthly averaged surface T_{soil} rising above 0°C (Figure 1b). And the subseasonal component of surface T_{soil} averaged over the ETP has the largest variance in the period of May and June (Figure 1c), which accounts for more than 65% of the total variance. As such, we focus on the early summer (May–June) to study the subseasonal variation of surface T_{soil}. To identify the predominant periodicity of the surface T_{soil} over the ETP, we made a multi-year power spectral analysis for the region-averaged T_{soil} during the 40 early summers of 1979–2018. As shown in Figure 1d, the QBW (9–30-day) is the dominant periodicity of the region-averaged T_{soil} over the ETP, which is very similar to the dominant subseasonal periodicity of the atmospheric signal.

Based on the selected 50 significant cases of surface T_{soil} QBW evolution (Figure S1b & Table S1 in Supporting Information S1) following the criteria introduced in Section 2.2, the spatial-temporal evolution of the surface T_{soil} QBW variation are explored along phase 1–8 through a phase composite technique. As shown in Figure 2a, the coldest QBW anomaly of surface T_{soil} occurs over the ETP at Phase 1. From Phase 1 to Phase 3, the QBW cold anomaly of surface T_{soil} weakens gradually. The surface T_{soil} warm anomaly appears at Phase 4 and reaches the maximum warming at Phase 5 for QBW. Afterward, the warm anomaly of surface T_{soil} is reduced and the cold anomaly appears again at Phases 7–8. As shown in Figure 2b, from Phase 1 to Phase 5 (this period is defined as "the surface soil warming phase" for brevity), the composite area-averaged total surface T_{soil} over the ETP warms by 3.3°C (yellow bars) while its QBW component warms by 1.8°C (red line), which suggests the overall contribution of surface T_{soil} QBW amplitude to the total amplitude is more than 50% and indeed significant over the ETP. Further calculation demonstrates that the ratio of the QBW T_{soil} warming to the total T_{soil} warming can
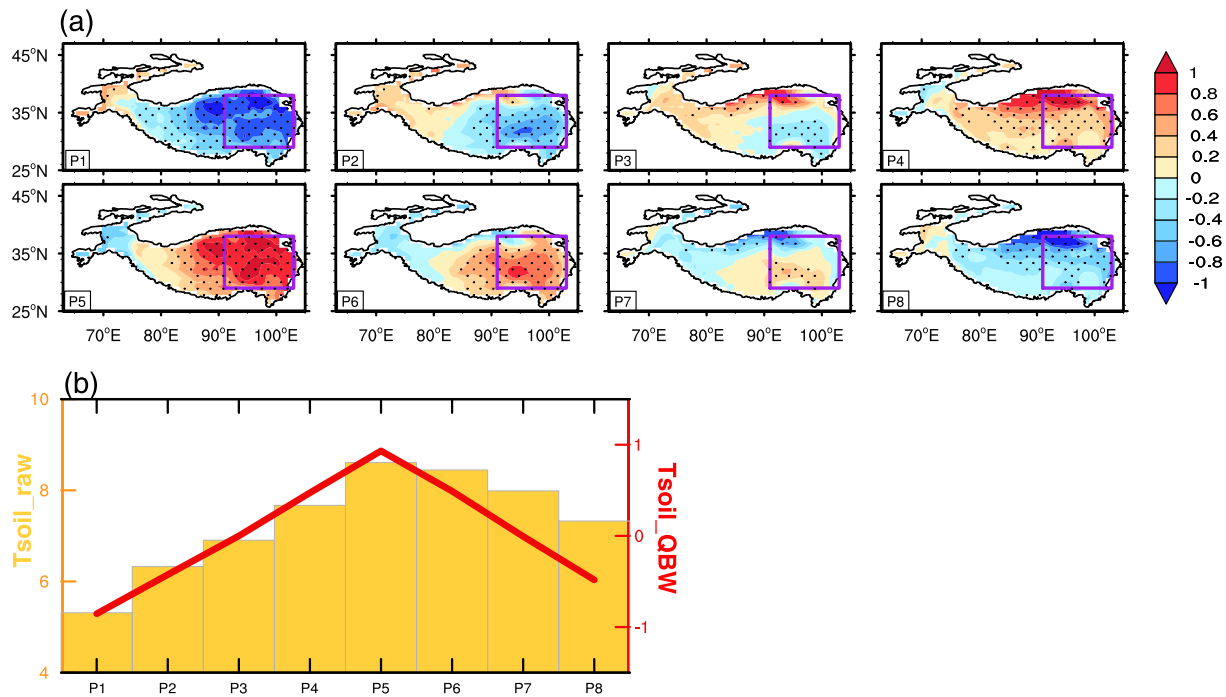
Figure 2. (a) Temporal evolution of surface T_{soil} (shading, °C) over the ETP on the 9–30-day timescale based on phase composite technique. Black dots denote the results significant at a 95% confidence level compared to the seasonal mean. Purple boxes denote the ETP region. (b) Temporal evolution of raw (left axis, yellow bars) and QBW (right axis, red line) surface T_{soil} (°C) averaged over the ETP. "P" means "phase".

be accounted for 51% on average in the selected events, which also indicates the QBW signal is crucial over the ETP in early summer.

3.2. QBW Warming of Surface T_{soil} Forced by QBW Atmospheric Waves

Since Many previous studies have reported that the atmosphere over the ETP exhibits an evident QBW signal that is associated with mid-latitude waves (e.g., Fujinami & Yasunari, 2004; Fujinami & Yasunari, 2009; Hu et al., 2016; Pan et al., 2013; Yang et al., 2017, more mentioned in Section 1), we intentionally investigate if the QBW warming of surface T_{soil} originates from the atmosphere QBW waves. Firstly, we examined the spatial-temporal evolution of the atmospheric QBW circulation in both the upper and middle troposphere (Figure 3). During the surface soil warming phase, a southeastward propagating QBW wave train starting from the Mediterranean is significantly identified roughly along the westerly jet in the mid-latitudes (30°–50°N) at the upper level (Figure 3a). And this wave train is characterized by a typical baroclinic structure (Figure 3b), which has been also reported in previous research (e.g., Wang & Duan, 2015; Yang et al., 2017; Zhang et al., 2014). Locally speaking, a significant positive anomalous vorticity center (cyclonic anomaly) first appears at 200 hPa over the ETP at Phase 1 (Figure 3a), which favors the upper-level convergence anomaly and induces the local anomalous subsidence. At Phases 2–3, with a well-established anticyclonic anomaly at 500 hPa over the ETP (Figures 3b and 4a), the anomalous subsidence (Figure 4b), reduced cloud cover (Figure 4c), and the positive downward solar radiation anomaly (Figure 4d) reach their extrema, which lead the maximum warming of the surface T_{soil} by three phases (about 6–9 days) at QBW timescale. Finally, the surface T_{soil} reaches its maximum warming at Phase 5. The lead-lag relationship between the surface T_{soil} and atmospheric variables (vorticity, vertical velocity, cloud cover, etc.) suggests that the QBW warming of the surface T_{soil} over the ETP is primarily forced by the QBW atmospheric circulation.
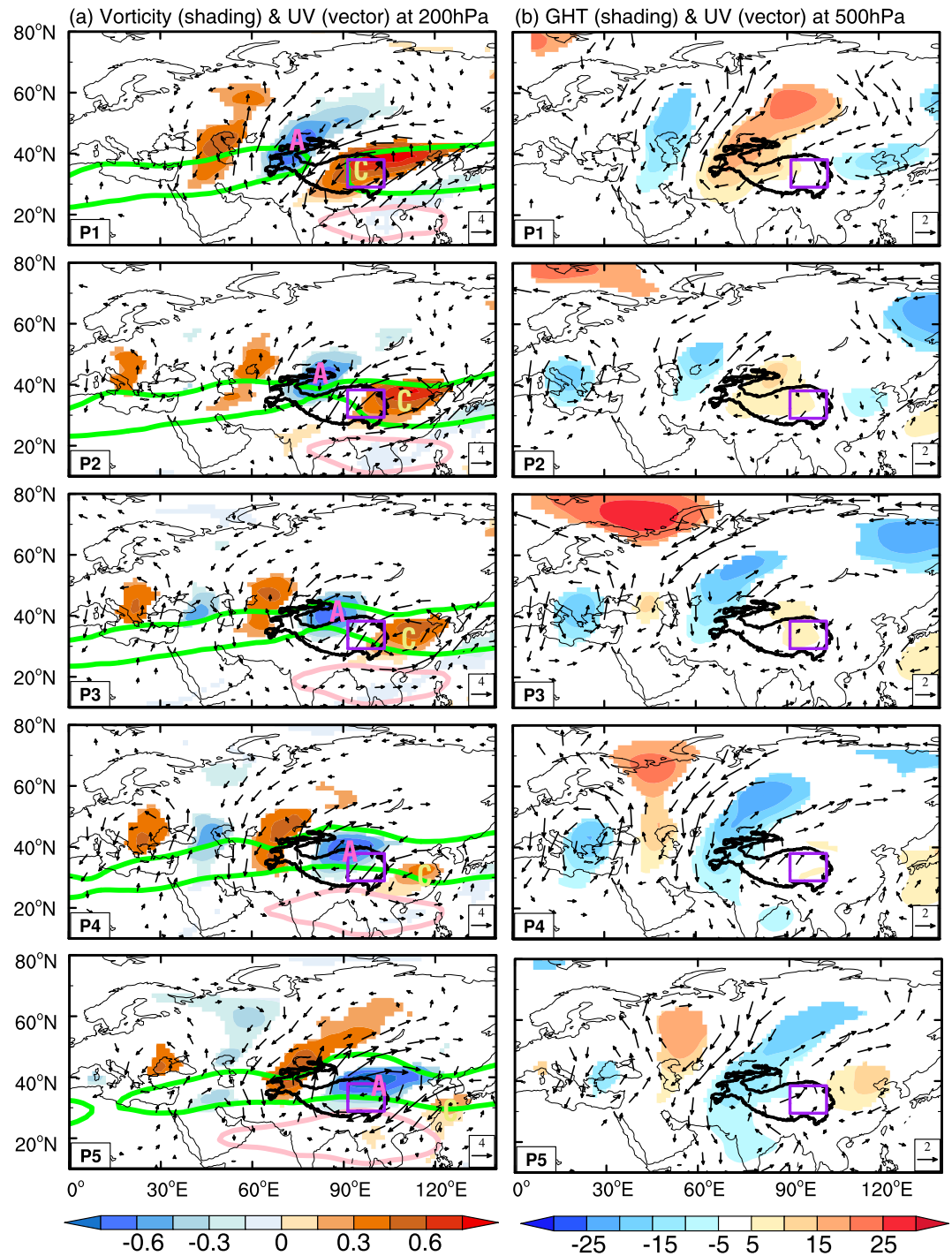
Figure 3. Temporal evolution of (a) 200 hPa winds (vectors, m s^{-1}) and vorticity (shading, 10^{-6} s^{-1}) anomalies on the 9–30-day time scale for phase 1–5 based on phase composite technique. Pink lines are the 200 hPa geopotential height contours at 12,490 gpm representing the location of the South Asian high. Green lines are the 200 hPa zonal winds contours at 25 m s^{-1} representing the westerly jet. (b) Same as (a), except for 500 hPa winds (vectors, m s^{-1}) and geopotential height anomalies (shading, gpm). "P" means "phase". "A" and "C" denote the center of anti-cyclone and cyclone, respectively. Purple boxes denote the ETP region. Only the results significant above 95% confidence level are shown.
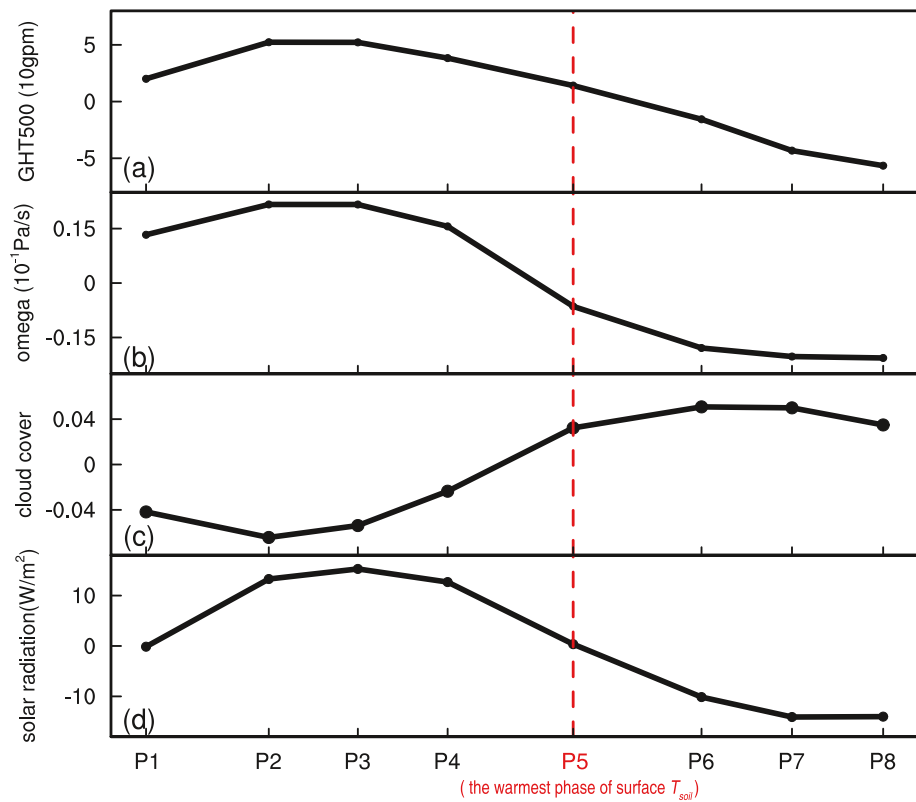
Figure 4. Temporal evolution of the averaged (a) geopotential height at 500 hPa, (b) the integral vertical velocity for 500–200 hPa, (c) cloud cover, and (d) solar radiation over the ETP at the 9–30-day timescale based on phase composite technique. "P" means "phase".

4. Warming Surface T_{soil} Enhances Precipitation Over the ETP in QBW Variation

Along with the QBW T_{soil} warming, however, we notice that the direction of anomalous surface sensible heat flux evidently shifts from downwards to upwards starting from Phase 4 and arrives at its positive peak value at the warmest phase of surface soil (Figure 5a). Meanwhile, instead of a subsidence anomaly, the ascending anomaly emerges in the near-surface troposphere over the ETP at Phase 5, extends upward, and reinforces at Phase 6 (Figure 5b). These changes near the peak warming phase of T_{soil} indicate that a significant impact of land on the atmosphere could occur, which may regulate the occurrence of the coming precipitation. As envisioned, the QBW peak value of the precipitation does occur at Phase 6, obviously lagging the peak warming phase of the surface T_{soil} by one phase (2–7 days) (Figure 6a). The lead-lag relationship between the surface T_{soil} and precipitation at QBW timescale over the ETP further suggests that the warming surface soil could play an important role in causing the local precipitation.

To further examine the feedback of warming soil to the atmosphere, we performed the simultaneous correlation analysis between the QBW surface T_{soil} and precipitation at each phase shown as in Figure 6b. Exceeding the 95% confidence level, significant positive correlations occur at the extreme phases of surface T_{soil} (Phases 1 and 5) and the phase of maximum precipitation (Phase 6), which suggests that the wet (dry) anomaly of the precipitation corresponds to the warming (cooling) surface soil at the extreme phase of QBW variation. Generally speaking, when the atmospheric role dominates, the positive precipitation anomaly could decrease surface T_{soil} through reducing the shortwave radiation thus the relationship between the anomalies of surface T_{soil} and precipitation exhibits a negative correlation. However, the present analysis shows a significant positive correlation between the QBW surface T_{soil} and precipitation, which indicates that the positive surface T_{soil} anomaly could increase the precipitation. This positive correlation relationship reflects the dominant role of land in physics, which is similar to that reflected in the atmosphere–warm ocean interaction presented by Wang et al. (2003). Accordingly, the significant positive correlation between the surface T_{soil} and precipitation here denotes that the land feedback dominates the land-air interaction at the extreme phase of surface T_{soil}. As shown in Figure 6c, we further detected
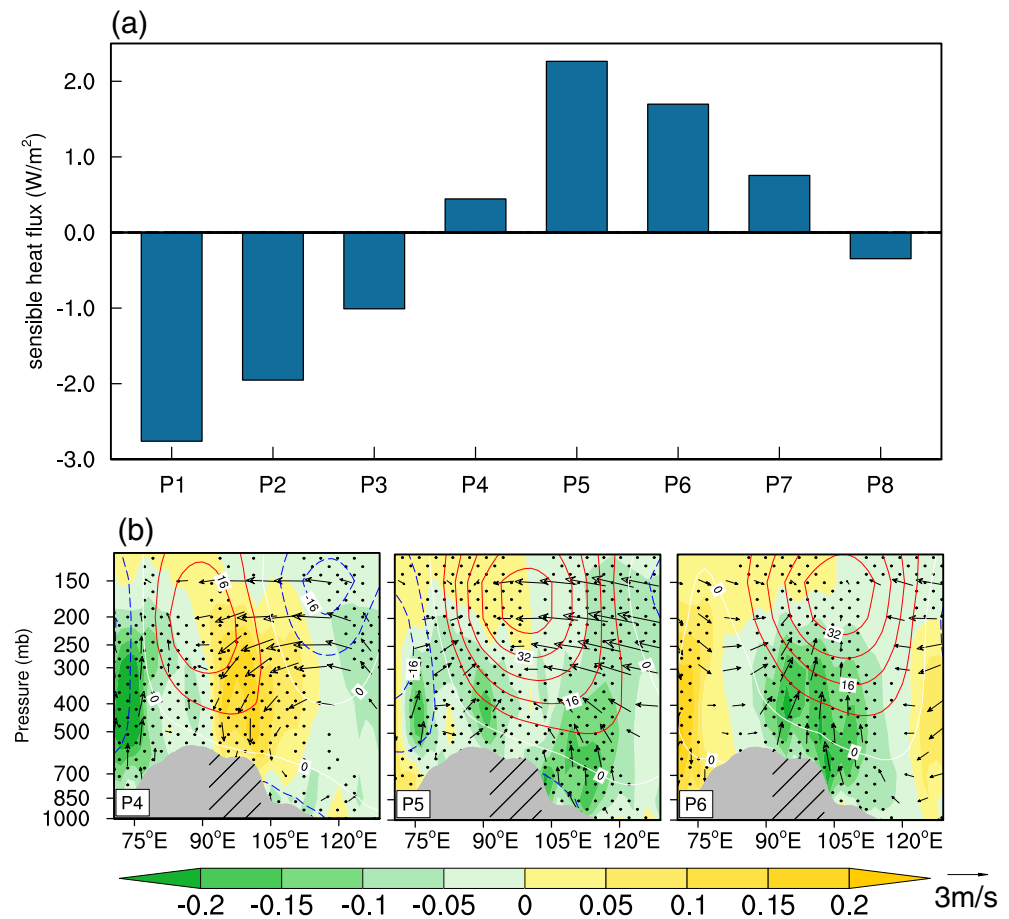
Figure 5. (a) Temporal evolution of the averaged sensible heat flux (W·m^{-2}) over the ETP at the 9–30-day timescale based on phase composite technique. (b) Longitudinal–pressure cross sections of composite results for 9–30-day phases averaged between 29° and 38°N. The shadings are the QBW filtered vertical velocity (10^{-1} Pa·s^{-1}, the negative value means ascending motion) and the contours are the QBW filtered geopotential height (gpm). The gray polygon denotes the topography and the shaded part with oblique lines represent ETP. Black dots denote the results significant at 95% confidence level. "P" means "phase".

the noticeable asymmetrical lead-lag relationship between the QBW filtered precipitation and surface T_{soil}. To be specific, a significant negative correlation between the anomalies of precipitation and surface T_{soil} from day −7 to −2 suggests that more precipitation could lead to the reduction of surface T_{soil}, reflecting the atmospheric role is dominated. In contrast, there is a significant positive correlation from day +1 to +5 when the anomalous surface T_{soil} leads the precipitation, revealing the predominant role of surface T_{soil} on the QBW precipitation. As noted above, the embodied asymmetry by the opposite sign of the correlation coefficients and the different lead/lag times indicates the surface T_{soil} could enhance precipitation at the QBW timescale.

According to the above-mentioned relationship that the anomalous positive precipitation lags the warming surface T_{soil} by one phase, we, therefore, conjecture that the warming surface T_{soil} over the ETP could exert significant thermal impact on the atmosphere through increasing upward sensible fluxes, ascending motion, and destabilizing the lower-level atmosphere, and eventually facilitate the precipitation. However, if we look back at the atmospheric condition, there is an anti-cyclonic anomaly at 200 hPa over the ETP at the peak phase, which favors the upper-level divergence anomaly and the local anomalous ascending motion. Influenced by an eastward cyclonic anomaly at 500 hPa, the ETP lower-level is under the control of a low-pressure anomaly after Phase 5 (Figure 4a & Figure S2 in Supporting Information S1), which also facilitates the development of convergence and ascending motion. This atmospheric circulation configuration after Phase 5 favors the occurrence of precipitation and the cooling of surface T_{soil}. Therefore, it is difficult to separate the effect of the atmosphere and land process only based on the observational analysis, since the precipitation seems to
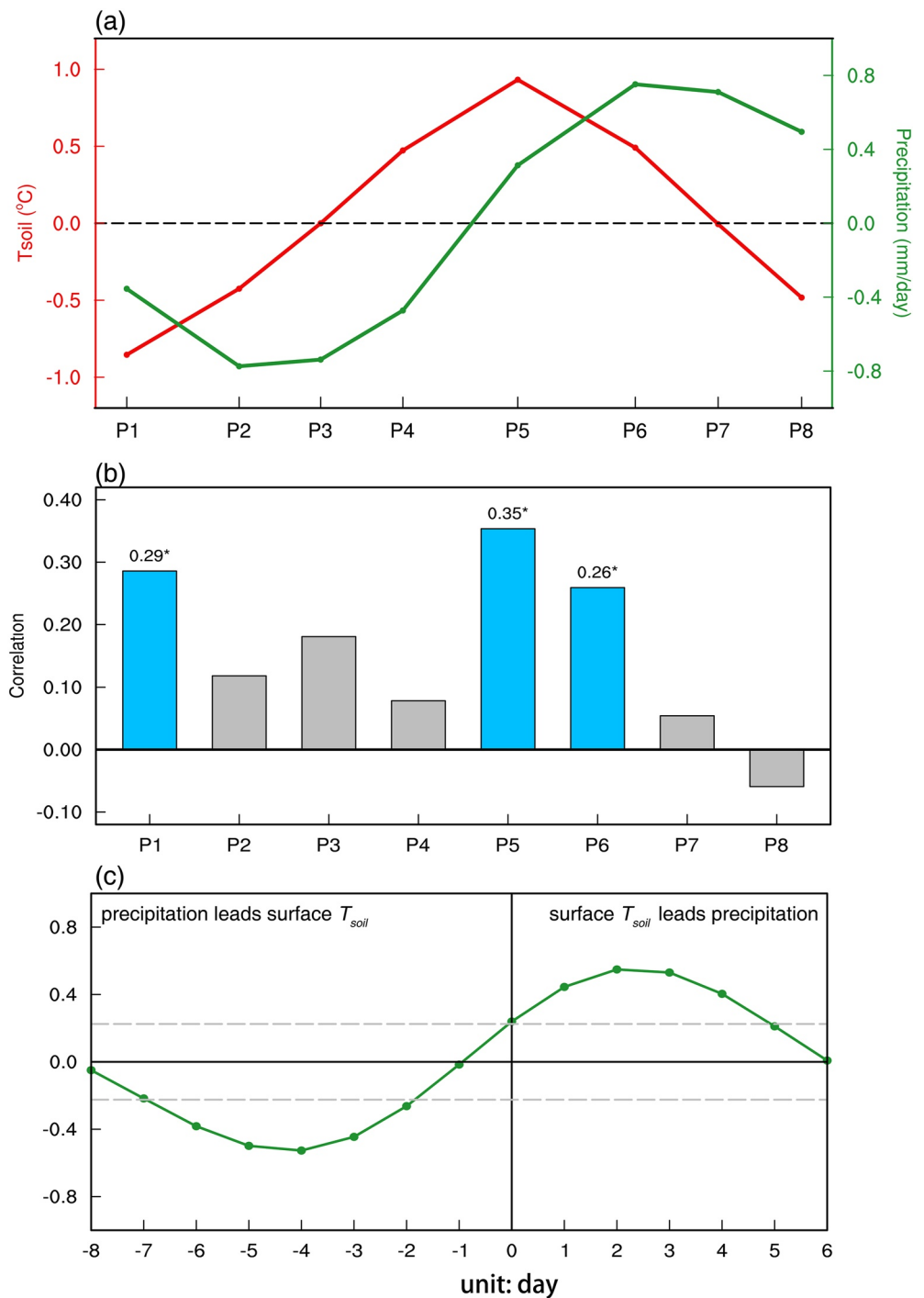
Figure 6. (a) Temporal evolution of the averaged surface T_{soil} (°C) and precipitation (mm day^{-1}) over the ETP at the 9-30-day timescale based on the phase composite technique. (b) The correlation coefficient between precipitation and temperature for each phase. Asterisks denote the results significant at a 95% confidence level. (c) lead-lag correlation coefficients between the surface T_{soil} and precipitation. The horizontal axis represents the lead/lag days. "P" means "phase".

occur when the cyclonic anomalies along the QBW waves invade over the ETP without land-air interaction. To further verify the role of the surface T_{soil} indicated from observational analysis, the sensitive numerical experiments using the WRF model were conducted to investigate the surface soil thermal effect quantitatively in the next section.
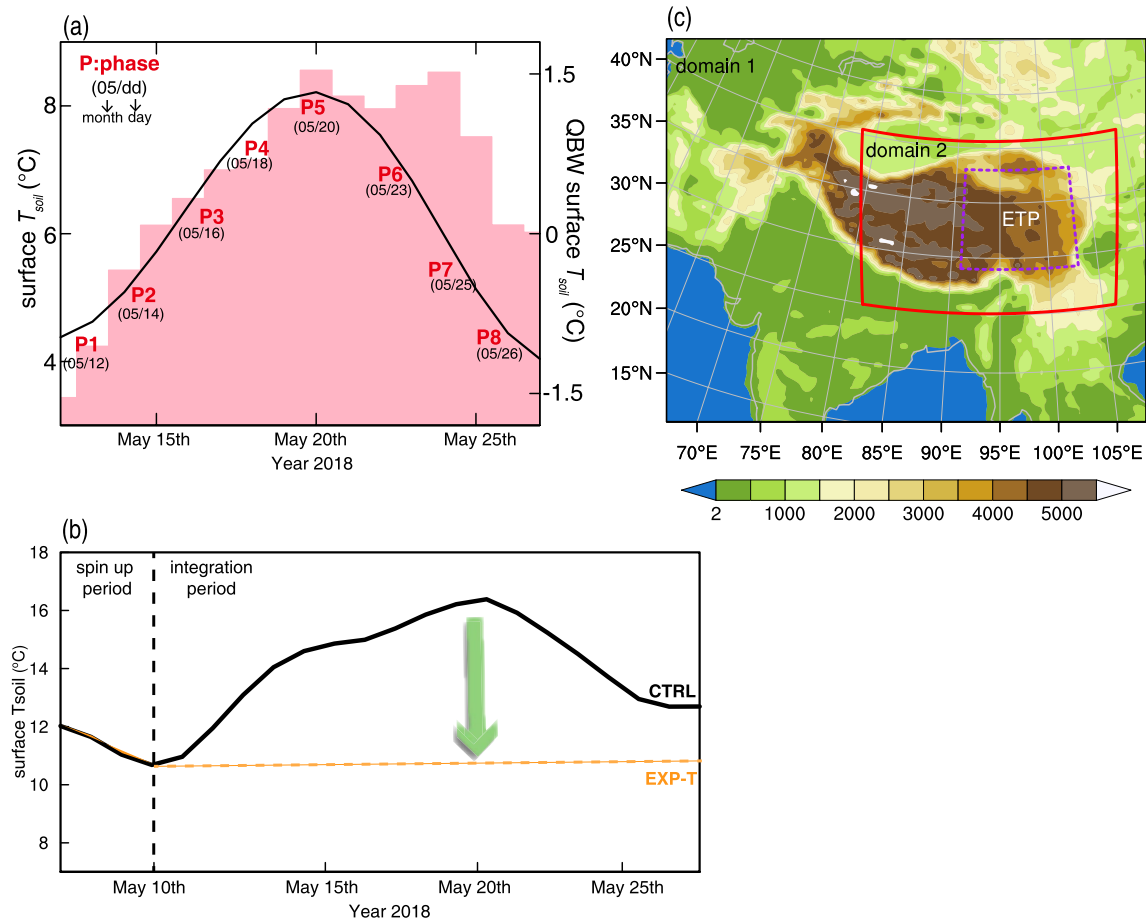
Figure 7. (a) Time series of raw (left axis, gy bars) and QBW (right axis, red line) surface T_{soil} (shading, °C) averaged over the ETP in May 2018. (b) Schematic diagram of the experimental design. (c) Topography over the WRF simulation area (shaded, m). The dashed purple box represents the ETP region.

5. Indispensable Roles of ETP Surface T_{soil} in Enhancing QBW Precipitation: A Numerical Study

5.1. Experimental Design

In order to examine the thermal effect of surface T_{soil} over the ETP on the precipitation anomaly, a typical QBW event that occurred on 12–28 May 2018 was selected from 50 typical events. As shown in Figure 7a, the surface T_{soil} arrived at its QBW peak phase on 20 May 2018, and the warming amplitude (12–20 May 2018) of 9–30-day filtered T_{soil} was up to 2.3°C, accounting for 45% of the real warming in observation. Aiming at the selected case, we conducted two ensemble WRF experiments named as the control run (CTRL) and sensitive run of surface T_{soil} (EXP-T), respectively. Here, the CTRL was conducted using actual initial and boundary forcing to simulate the QBW variation, whereas the EXP-T re-initialized the forcing of T_{soil} to the initial state (00hr 12 May 2018) every 3 hr so as to eliminate the QBW fluctuation of T_{soil} (Figure 7b). All the physical parameterization options for both the CTRL and EXP-T remain the same, and the modeling details have been described in Section 2.2.

As shown in Figure 7c, two nested grids with a horizontal grid spacing of 30 km (domain 1) and 10 km (domain 2) were used. The outer domain had 160 (zonal) × 128 (meridional) grid points, covering the region roughly from 10 to 42°N and 68 to 107°E, and the inner domain covered most parts of TP and the adjacent region with 253 grid points along the east-west direction and 175 along the north-south direction. All the integrations were initiated on 7 May 2018 and ended on 28 May 2018. In order to balance the forcing dynamically, the first three days (7–9 May 2018) were considered to be the spin-up period. Each ensemble experiment has five members with different start times using the time-lagged technique (Qi et al., 2019; Xu et al., 2014) to reduce the possible influence of the initial condition, and the ensemble mean of the outputs from 10 May to 28 May 2018 were analyzed.
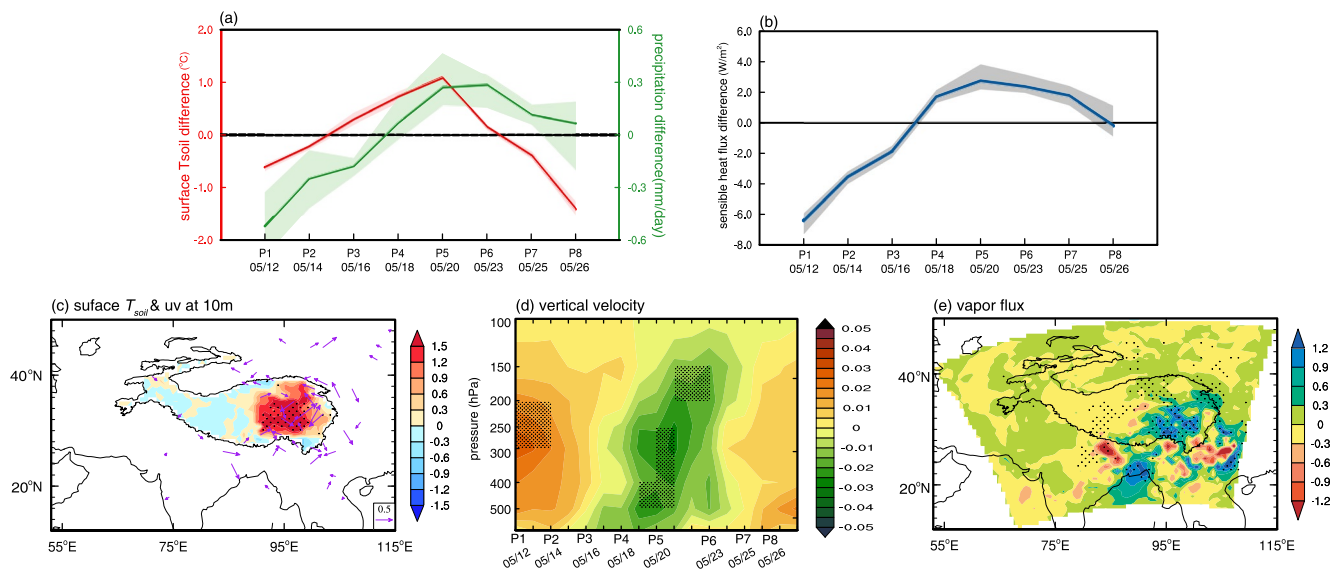
Figure 8. Temporal evolution of (a) surface T_{soil} (°C) and precipitation (mm·day^{-1}), (b) sensible heat flux (W·m^{-2}) averaged over the ETP in May 2018. The lines denote the ensemble mean of the control (sensitive) run. The shaded represents the range of ensemble members. (c) The difference of surface winds (vectors, m·s^{-1}) and T_{soil} (shading, °C) between CTRL and EXP-T at Phase 5. (d) The difference in vertical velocity (Pa·s^{-1}, the negative value means ascending motion) between CTRL and EXP-T averaged over the ETP in May 2018. (e) The difference of surface vapor flux (shading, 10^{-2} kg·cm^{-1}·s^{-1}·hPa^{-1}) between CTRL and EXP-T at Phase 5. Black dots denote the results significant at 95% confidence level.

5.2. Numerical Results

Compared with the observational examination shown in Figure 7a, the QBW development of the selected event is well simulated in CTRL (Figure 7b). To distinguish the role of the ETP surface T_{soil} on the anomalous precipitation at the QBW timescale, the differences between the CTRL and EXP_T runs are exhibited in Figure 8. Firstly, shown as in Figure 8a, the difference in the surface T_{soil} between CTRL and EXP-T features an obvious QBW cycle peaking at Phase 5, which confirms the QBW signal of surface T_{soil} has been completely removed in the EXP-T. Second, the maximum difference of surface T_{soil} at Phase 5 corresponds to the largest difference of the responded precipitation at Phase 6, which is exactly consistent with the observed lag relationship (Figure 6a). Compared to the total precipitation in EXP-T, the rainfall in CTRL is significantly intensified by nearly 50% with the QBW variation of surface T_{soil}, which suggests that the QBW warming of surface T_{soil} over the ETP remarkably increases the precipitation intensity.

To explore the mechanism of how the warming surface soil enhances precipitation at the QBW timescale, the differences between the CTRL and EXP-T were also calculated for the sensible heat flux, surface T_{soil}, surface wind, vertical velocity, and surface vapor flux. First, the difference in upward sensible heat flux reaches the largest at Phase 5, showing an in-step change with the QBW surface T_{soil} (Figure 8b). With the QBW variation of surface T_{soil}, the upwards sensible heat flux is increased by 11% at Phase 5. Meanwhile, along with the QBW surface T_{soil} variation in the CTRL, a clear cyclonic anomaly is detected over the ETP near the surface troposphere at Phase 5 (Figure 8c), and accordingly, an evident ascending anomaly appears at Phase 5 in the troposphere (500–150 hPa) (Figure 8d). Consistent with the above change of dynamical fields, the lower-level water vapor flux is increased by 23.1% at Phase 5 (Figure 8e). The numerical results indicate that the ETP warming surface T_{soil} could significantly increase the local upward sensible heat flux and intensify anomalous ascending motion, which enhances the convergence of water vapor and eventually increases the local precipitation at the QBW timescale, which verifies the aforementioned hypothesis in Section 4.

6. Discussion and Conclusion

6.1. Discussion

Note that the soil moisture (M_{soil}) as with the T_{soil} is also a key land factor in land-air interactions, many prior studies have investigated the roles of M_{soil} over the TP (e.g., Talib et al., 2021; Yang & Wang, 2019). Given that the

anomalous signals of M_{soil} tend to be more persistent than T_{soil} (Koster & Suarez, 2001; Yeh et al., 1984), current studies about TP M_{soil} and its associated land-air interaction mainly concentrated on the remote effect at seasonal/interannual timescale (e.g., Xue et al., 2018; Zhou et al., 2002). For example, Yang and Wang (2019) reported that positive M_{soil} anomalies over the TP during the spring can enhance the summer precipitation anomalies in eastern China, and this relationship even can be retrospect to the anomalous M_{soil} conditions in the preceding autumn and winter. However, whether the M_{soil} over the ETP plays a comparable role with the T_{soil} at a subseasonal time scale remains unclear.

To clarify the question, an additional experiment named sensitive run for M_{soil} (EXP-M) was designed to identify the role of the surface M_{soil} in this precipitation event. First, we found the QBW signal is not evident in the M_{soil} variation (red line in Figure 9a). With the increase of surface M_{soil}, the upward sensible heat flux decreases by around 11% on average in the EXP-M (Figure 9b). There are no significant differences in both precipitation and low-level circulation with and without the change of the surface M_{soil} (Figure 9c and 9d). Though the ascending motion is enhanced at Phase 5 in the troposphere (500–150 hPa) with the increase of the surface M_{soil}, the increased intensity of anomalous ascending and moisture is much weaker than that shown in EXP-T (Figures 9e and 9f). Therefore, the effect of surface M_{soil} on the local precipitation variation is much smaller than T_{soil} on the subseasonal time scale.

The slight role of the M_{soil} in the precipitation subseasonal variation on the ETP during boreal summer is essentially due to the small contribution from the local evaporation to the subseasonal rainfall because the subseasonal rainfall anomaly over the ETP mainly comes from the subseasonal moisture convergence from the surrounding regions of TP. Different from the long-term time scale including interannual and global-change time scale, the surface thermal effect among land-air interaction is the most important for modulating the subseasonal rainfall variation over the ETP. Therefore, increasing the accuracy of the surface soil thermal condition during the process of initialization and integration is crucial for improving rainfall subseasonal prediction, especially for the events with large rainfall amounts as selected in this study. To avoid cherry-picking from one case, another case is also examined to confirm the result (Figure S3–4 in Supporting Information S1).

Additionally, to examine whether the philosophy found here can be applied in other seasons and other regions, we briefly choose the late summer (July–August) and western TP region (29°–38°N, 90°–101°E) as examples for comparison. However, the above-mentioned significant lead-lag correlation coefficients between the surface T_{soil} and precipitation do not occur over the western TP and in late summer (Figure S5 in Supporting Information S1). Therefore, this study highlighted the importance of surface T_{soil} over the ETP in regulating the anomalous atmospheric circulation during the early summer, which is regional dependent and worthwhile to be examined in other regions of the globe in future work.

7. Conclusion

Based on station and reanalysis datasets of 1979–2018, this study ascertains the evident QBW variation (9–30 days) of surface T_{soil} over the ETP during the early summer (May–June), which is associated with southeastward mid-latitude QBW waves in the mid-to-upper troposphere. In turn, the QBW variation of soil heating over the ETP can enhance the lower-level convective static instability via the increased sensible heat flux and accumulated ascending motion, resulting in a significant enhancement of precipitation. The numerical results further demonstrate the significant T_{soil} effect on enhancing the local cyclonic and rainfall anomaly through increasing sensible heat flux, the ascending motion, and water vapor convergence at the QBW time scale. Numerical experiments also show that T_{soil} feedback to the atmosphere is more significant than M_{soil} over the ETP in subseasonal land-air interactions. This study highlighted the importance of T_{soil} over the ETP in regulating the anomalous atmospheric circulation, indicating that overlooking the role of QBW variation of T_{soil} may lead to an underestimation of precipitation intensity. These findings not only offer a reference for evaluating how well is the coupled land-air process represented in subseasonal prediction models but also suggest that a better simulation of the impact of T_{soil} on the atmosphere at QBW timescales is crucial for improving subseasonal prediction.

This work mainly investigated the effect of the subseasonal warming of the surface soil on the precipitation over the ETP during early summer, it would be interesting to determine whether the role is symmetric for the period of subseasonal cooling of the surface soil in the near future. Besides, due to the complex and diverse landforms over the ETP, the effect of land cover and soil texture on the surface T_{soil} was not taken into account both in
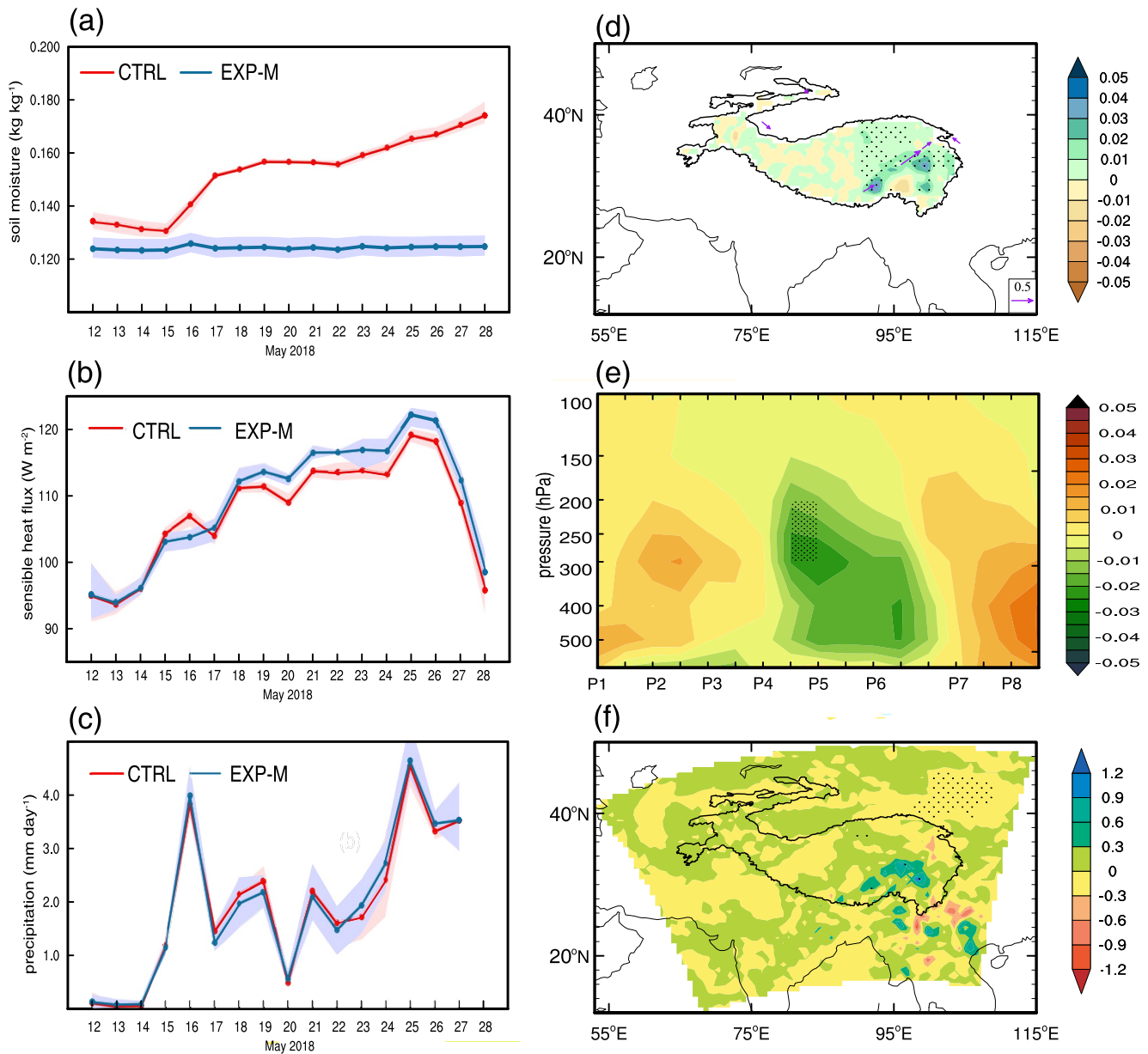
Figure 9. Temporal evolution of (a) surface soil moisture (kg·kg^{-1}) (b) sensible heat flux (W·m^{-2}), and (c) precipitation (mm·day^{-1}) averaged over the ETP in May 2018. The red (blue) lines denote the ensemble mean of CTRL (EXP-M). The shaded represents the range of ensemble members. (d) The difference of surface winds (vectors, m·s^{-1}) and surface soil moisture (shading, kg·kg^{-1}) between CTRL and EXP-M at Phase 5. (e) the difference in vertical velocity (Pa·s^{-1}, the negative value means ascending motion) between CTRL and EXP-M averaged over the ETP in May 2018. (f) The difference of surface vapor flux (shading, 10^{-2} kg·cm^{-1}·s^{-1} hPa^{-1}) between CTRL and EXP-M at Phase 5. Black dots denote the results significant at 95% confidence level.

the observational study and numerical simulations. Therefore, the uncertainties from the soil data and WRF model also needs further exploration in the future study.

Data Availability Statement

The ERA-Interim data and gauge station precipitation data can be accessed on https://apps.ecmwf.int/datasets/ and http://data.cma.cn, respectively. The observational station dataset of soil temperature over the Tibetan Plateau can be retrieved from http://data.tpdc.ac.cn/en/.

References

Amenu, G. G., Kumar, P., & Liang, X. Z. (2005). Interannual variability of deep-layer hydrologic memory and mechanisms of its influence on surface energy fluxes. *Journal of Climate*, *18*(23), 5024–5045. https://doi.org/10.1175/jcli3590.1

Bingham, C., Godfrey, M. D., & Tukey, J. W. (1967). Modern techniques of power spectrum estimation. *IEEE Transactions on Audio and Electroacoustics*, *AU15*(2), 56–66. https://doi.org/10.1109/tau.1967.1161895

Bloomfield, P. (2000). *Fourier analysis of time series: An introduction* (2nd ed.). Wiley.

Deardorff, J. W. (1978). Efficient prediction of ground surface-temperature and moisture, with inclusion of a layer of vegetation. *Journal of Geophysical Research*, *83*(NC4), 1889–1903. https://doi.org/10.1029/JC083iC04p01889

Dee, D. P., Uppala, S. M., Simmons, A. J., Berrisford, P., Poli, P., Kobayashi, S., et al. (2011). The ERA-snterim reanalysis: Configuration and performance of the data assimilation system. *Quarterly Journal of the Royal Meteorological Society*, *137*(656), 553–597. https://doi.org/10.1002/qj.828

Delworth, T. L., & Manabe, S. (1988). The influence of potential evaporation on the variabilities of simulated soil wetness and climate. *Journal of Climate*, *1*(5), 523–547. https://doi.org/10.1175/1520-0442(1988)001<0523:tiopeo>2.0.co;2

Dirmeyer, P. A., Halder, S., & Bombardi, R. (2018). On the harvest of predictability from land states in a global forecast model. *Journal of Geophysical Research-Atmospheres*, *123*(23), 13111–13127. https://doi.org/10.1029/2018jd029103

Duan, A., Wu, G., Liu, Y., Ma, Y., & Zhao, P. (2012). Weather and climate effects of the Tibetan Plateau. *Advances in Atmospheric Sciences*, *29*(5), 978–992. https://doi.org/10.1007/s00376-012-1220-y

Dugam, S. S., Bansod, S. D., & Kakade, S. B. (2009). Pre-monsoon zonal wind index over Tibetan Plateau and sub-seasonal Indian summer monsoon rainfall variability. *Geophysical Research Letters*, *36*(11), L11809. https://doi.org/10.1029/2009gl038207

Feng, L., & Zhou, T. J. (2012). Water vapor transport for summer precipitation over the Tibetan Plateau: Multidata set analysis. *Journal of Geophysical Research*, *117*(D20). https://doi.org/10.1029/2011jd017012

Fu, Y. F., Ma, Y. M., Zhong, L., Yang, Y. J., Guo, X. L., Wang, C. H., et al. (2020). Land-surface processes and summer-cloud-precipitation characteristics in the Tibetan plateau and their effects on downstream weather: A review and perspective. *National Science Review*, *7*(3), 500–515. https://doi.org/10.1093/nsr/nwz226

Fujinami, H., & Yasunari, T. (2004). Submonthly variability of convection and circulation over and around the Tibetan Plateau during the boreal summer. *Journal of the Meteorological Society of Japan*, *82*(6), 1545–1564. https://doi.org/10.2151/jmsj.82.1545

Fujinami, H., & Yasunari, T. (2009). The effects of midlatitude waves over and around the Tibetan Plateau on submonthly variability of the East Asian summer monsoon. *Monthly Weather Review*, *137*(7), 2286–2304. https://doi.org/10.1175/2009mwr2826.1

Gao, M., Yang, J., Wang, B., Zhou, S., Gong, D., & Kim, S.-J. (2018). How are heat waves over Yangtze River valley associated with atmospheric quasi-biweekly oscillation? *Climate Dynamics*, *51*(11–12), 4421–4437. https://doi.org/10.1007/s00382-017-3526-z

Gao, Y., Li, K., Chen, F., Jiang, Y., & Lu, C. (2015). Assessing and improving Noah-MP land model simulations for the central Tibetan Plateau. *Journal of Geophysical Research-Atmospheres*, *120*(18), 9258–9278. https://doi.org/10.1002/2015jd023404

Gilman, D. L., Fuglister, F. J., & Mitchell, J. M. (1963). On the power spectrum of red noise. *Journal of the Atmospheric Sciences*, *20*(2), 182–184. https://doi.org/10.1175/1520-0469(1963)020<0182:otpson>2.0.co;2;2

Glotfelty, T., Alapaty, K., He, J., Hawbecker, P., Song, X., & Zhang, G. (2019). The weather research and forecasting model with aerosol-cloud interactions (WRF-ACI): Development, evaluation, and initial application. *Monthly Weather Review*, *147*(5), 1491–1511. https://doi.org/10.1175/mwr-d-18-0267.1

Guo, W. D., Sun, S. F., & Qian, Y. F. (2002). Case analyses and numerical simulation of soil thermal impacts on land surface energy budget based on an off-line land surface model. *Advances in Atmospheric Sciences*, *19*(3), 500–512. https://doi.org/10.1007/s00376-002-0082-0

Hong, S. –Y., & Lim, J. –O. J. (2006). The WRF single–moment 6–class microphysics scheme (WSM6). *Journal of the Korean Meteorological Society*, *42*, 129–151.

Hong, S.-Y., Noh, Y., & Dudhia, J. (2006). A new vertical diffusion package with an explicit treatment of entrainment processes. *Monthly Weather Review*, *134*(9), 2318–2341. https://doi.org/10.1175/mwr3199.1

Hu, W., Duan, A., Li, Y., & He, B. (2016). The intraseasonal oscillation of eastern Tibetan Plateau precipitation in response to the summer Eurasian wave train. *Journal of Climate*, *29*(20), 7215–7230. https://doi.org/10.1175/jcli-d-15-0620.1

Iacono, M. J., Delamere, J. S., Mlawer, E. J., Shephard, M. W., Clough, S. A., & Collins, W. D. (2008). Radiative forcing by long-lived greenhouse gases: Calculations with the AER radiative transfer models. *Journal of Geophysical Research*, *113*(D13), D13103. https://doi.org/10.1029/2008jd009944

Jimenez, P. A., Dudhia, J., Gonzalez-Rouco, J. F., Navarro, J., Montavez, J. P., & Garcia-Bustamante, E. (2012). A revised scheme for the WRF surface layer formulation. *Monthly Weather Review*, *140*(3), 898–918. https://doi.org/10.1175/mwr-d-11-00056.1

Koster, R. D., Dirmeyer, P. A., Guo, Z. C., Bonan, G., Chan, E., Cox, P., et al. (2004). Regions of strong coupling between soil moisture and precipitation. *Science*, *305*(5687), 1138–1140. https://doi.org/10.1126/science.1100217

Koster, R. D., & Suarez, M. J. (2001). Soil moisture memory in climate models. *Journal of Hydrometeorology*, *2*(6), 558–570. https://doi.org/10.1175/1525-7541(2001)002<0558:smmicm>2.0.co;2;2

Li, Q., Xue, Y., & Liu, Y. (2021). Impact of frozen soil processes on soil thermal characteristics at seasonal to decadal scales over the Tibetan Plateau and North China. *Hydrology and Earth System Sciences*, *25*(4), 2089–2107. https://doi.org/10.5194/hess-25-2089-2021

Li, W., Guo, W., Qiu, B., Xue, Y., Hsu, P.-C., & Wei, J. (2018). Influence of Tibetan Plateau snow cover on East Asian atmospheric circulation at medium-range time scales. *Nature Communications*, *9*(1), 4243. https://doi.org/10.1038/s41467-018-06762-5

Liu, Y., Hoskins, B., & Blackburn, M. (2007). Impact of Tibetan orography and heating on the summer flow over Asia. *Journal of the Meteorological Society of Japan*, *85B*, 1–19. https://doi.org/10.2151/jmsj.85B.1

Liu, Y., Xue, Y., Li, Q., Lettenmaier, D., & Zhao, P. (2020). Investigation of the variability of near-surface temperature anomaly and its causes over the Tibetan Plateau. *Journal of Geophysical Research-Atmospheres*, *125*(19). https://doi.org/10.1029/2020jd032800

Luo, S., Wang, J., Pomeroy, J. W., & Lyu, S. (2020). Freeze-thaw changes of seasonally frozen ground on the Tibetan Plateau from 1960 to 2014. *Journal of Climate*, *33*(21), 9427–9446. https://doi.org/10.1175/jcli-d-19-0923.1

Ma, Y., Menenti, M., & Feddes, R. (2010). Parameterization of heat fluxes at heterogeneous surfaces by integrating satellite measurements with surface layer and atmospheric boundary layer observations. *Advances in Atmospheric Sciences*, *27*(2), 328–336. https://doi.org/10.1007/s00376-009-9024-4

Mariotti, A., Ruti, P. M., & Rixen, M. (2018). Progress in subseasonal to seasonal prediction through a joint weather and climate community effort. *NPJ Climate and Atmospheric Science*, *1*, 4. https://doi.org/10.1038/s41612-018-0014-z

Maussion, F., Scherer, D., Moelg, T., Collier, E., Curio, J., & Finkelnburg, R. (2014). Precipitation seasonality and variability over the Tibetan Plateau as resolved by the high Asia reanalysis. *Journal of Climate*, *27*(5), 1910–1927. https://doi.org/10.1175/jcli-d-13-00282.1

Mihalakakou, G. (2002). On estimating soil surface temperature profiles. *Energy and Buildings*, *34*(3), 251–259. https://doi.org/10.1016/s0378-7788(01)00089-5

Pan, W., Mao, J., & Wu, G. (2013). Characteristics and mechanism of the 10–20-day oscillation of spring rainfall over Southern China. *Journal of Climate*, *26*(14), 5072–5087. https://doi.org/10.1175/JCLI-D-12-00618.1

Pyper, B. J., & Peterman, R. M. (1998). Comparison of methods to account for autocorrelation in correlation analyses of fish data. *Canadian Journal of Fisheries and Aquatic Sciences*, *55*(9), 2127–2140. https://doi.org/10.1139/f98-104

Qi, X., Yang, J., Gao, M., Yang, H., & Liu, H. (2019). Roles of the tropical/extratropical intraseasonal oscillations on generating the heat wave over Yangtze river valley: A numerical study. *Journal of Geophysical Research-Atmospheres*, *124*(6), 3110–3123. https://doi.org/10.1029/2018jd029868

Qian, Y., & Shen, J. (1990). Effect of Tibetan Plateau on short-range numerical weather prediction. *Scientia Meteorologica Sinica*, *10*(2), 129–138.

Qiu, Y., Feng, J., Wang, J., Xue, Y., & Xu, Z. (2021). Memory of land surface and subsurface temperature (LST/SUBT) initial anomalies over Tibetan Plateau in different land models. *Climate Dynamics*. https://doi.org/10.1007/s00382-021-05937-z

Schiemann, R., Luthi, D., Vidale, P. L., & Schar, C. (2008). The precipitation climate of Central Asia - Intercomparison of observational and numerical data sources in a remote semiarid region. *International Journal of Climatology*, *28*(3), 295–314. https://doi.org/10.1002/joc.1532

Seneviratne, S. I., Luethi, D., Litschi, M., & Schaer, C. (2006). Land-atmosphere coupling and climate change in Europe. *Nature*, *443*(7108), 205–209. https://doi.org/10.1038/nature05095

Simmons, A., Uppala, S., Dee, D., & Kobayashi, S. (2007). ERA interim: New ECMWF reanalysis products from 1989 onwards. *ECMWF Newsletter*, *110*, 25–35. https://doi.org/10.21957/pocnex23c6

Skamarock, W. C., Klemp, J. B., Dudhia, J., Gill, D. O., Barker, D. M., Wang, W., & Powers, J. G. (2008). *A description of the advanced research WRF version 3*. NCAR Technical Note NCAR/TN-475+STR. https://doi.org/10.5065/D68S4MVH

Su, Z., Wen, J., Dente, L., Van der Velde, R., Wang, L., Ma, Y., et al. (2011). The Tibetan Plateau observatory of plateau scale soil moisture and soil temperature (Tibet-Obs) for quantifying uncertainties in coarse resolution satellite and model products. *Hydrology and Earth System Sciences*, *15*(7), 2303–2316. https://doi.org/10.5194/hess-15-2303-2011

Talib, J., Taylor, C. M., Duan, A., & Turner, A. G. (2021). Intraseasonal soil moisture-atmosphere feedbacks on the Tibetan Plateau circulation. *Journal of Climate*, *34*(5), 1789–1807. https://doi.org/10.1175/jcli-d-20-0377.1

Tao, S. Y., & Ding, Y. H. (1981). Observational evidence of the influence of the Qinghai-Xizang (Tibet) Plateau on the occurrence of heavy rain and severe convective storms in China. *Bulletin of the American Meteorological Society*, *62*(1), 23–30. https://doi.org/10.1175/1520-0477(1981)062<0023:oeotio>2.0.co;2;2

Tewari, M., Chen, F., Wang, W., Dudhia, J., LeMone, M. A., Mitchell, K., et al. (2004). Implementation and verification of the unified NOAH land surface model in the WRF model. *20th Conference on Weather Analysis and Forecasting/16th Conference on Numerical Weather Prediction*, 11–15.

Ullah, W., Wang, G., Gao, Z., Hagan, D. F. T., Bhatti, A. S., & Zhua, C. (2021). Observed linkage between Tibetan Plateau soil moisture and South Asian summer precipitation and the possible mechanism. *Journal of Climate*, *34*(1), 361–377. https://doi.org/10.1175/jcli-d-20-0347.1

Ullah, W., Wang, G., Gao, Z., Hagan, D. F. T., & Lou, D. (2018). Comparisons of remote sensing and reanalysis soil moisture products over the Tibetan Plateau, China. *Cold Regions Science and Technology*, *146*, 110–121. https://doi.org/10.1016/j.coldregions.2017.12.003

Wan, B., Gao, Z., Chen, F., & Lu, C. (2017). Impact of Tibetan Plateau surface heating on persistent extreme precipitation events in Southeastern China. *Monthly Weather Review*, *145*(9), 3485–3505. https://doi.org/10.1175/mwr-d-17-0061.1

Wang, B., Wu, R. G., & Li, T. (2003). Atmosphere-warm ocean interaction and its impacts on Asian-Australian monsoon variation. *Journal of Climate*, *16*(8), 1195–1211. https://doi.org/10.1175/1520-0442(2003)16<1195:aoiaii>2.0.co;2;2

Wang, M., & Duan, A. (2015). Quasi-biweekly oscillation over the Tibetan Plateau and its link with the Asian summer monsoon. *Journal of Climate*, *28*(12), 4921–4940. https://doi.org/10.1175/jcli-d-14-00658.1

Wang, Y., Chen, L., He, J., & Zhang, B. (2009). Effect of summer heat source low-frequency oscillation over the Tibetan Plateau on precipitation in Eastern China (in Chinese). *Journal of Applied Meteorolgical Science*, *20*(4), 419–427.

Webster, P. J., Magana, V. O., Palmer, T. N., Shukla, J., Tomas, R. A., Yanai, M., & Yasunari, T. (1998). Monsoons: Processes, predictability, and the prospects for prediction. *Journal of Geophysical Research*, *103*(C7), 14451–14510. https://doi.org/10.1029/97jc02719

Wei, J., & Dirmeyer, P. A. (2010). Toward understanding the large-scale land-atmosphere coupling in the models: Roles of different processes. *Geophysical Research Letters*, *37*(19), a–n. https://doi.org/10.1029/2010gl044769

Xu, X. D., Zhou, M. Y., Chen, J. Y., Bian, L. G., Zhang, G. Z., Liu, H. Z., et al. (2002). A comprehensive physical pattern of land-air dynamic and thermal structure on the Qinghai-Xizang Plateau. *Science in China - Series D: Earth Sciences*, *45*(7), 577–594. https://doi.org/10.1360/02yd9060

Xu, Y., Li, T., & Peng, M. (2014). Roles of the synoptic-scale wave train, the intraseasonal oscillation, and high-frequency Eddies in the Genesis of Typhoon Manyi (2001). *Journal of the Atmospheric Sciences*, *71*(10), 3706–3722. https://doi.org/10.1175/jas-d-13-0406.1

Xue, Y., Diallo, I., Boone, A. A., Yao, T., Zhang, Y., Zeng, X., et al. (2022). Spring land temperature in Tibetan Plateau and global-scale summer precipitation – Initialization and improved prediction. *Bulletin of the American Meteorological Society*. (published online ahead of print 2022). https://doi.org/10.1175/BAMS-D-21-0270.1

Xue, Y., Diallo, I., Li, W., Neelin, J. D., Chu, P. C., Vasic, R., et al. (2018). Spring land surface and subsurface temperature anomalies and subsequent downstream late spring-summer droughts/floods in North America and East Asia. *Journal of Geophysical Research-Atmospheres*, *123*(10), 5001–5019. https://doi.org/10.1029/2017jd028246

Xue, Y., Yao, T., Boone, A. A., Diallo, I., Liu, Y., Zeng, X., et al. (2021). Impact of initialized land surface temperature and snowpack on subseasonal to seasonal prediction project, phase I (LS4P-I): Organization and experimental design. *Geoscientific Model Development*, *14*(7), 4465–4494. https://doi.org/10.5194/gmd-14-4465-2021

Yang, J., Bao, Q., Wang, B., Gong, D.-Y., He, H., & Gao, M.-N. (2014). Distinct quasi-biweekly features of the subtropical East Asian monsoon during early and late summers. *Climate Dynamics*, *42*(5–6), 1469–1486. https://doi.org/10.1007/s00382-013-1728-6

Yang, J., Bao, Q., Wang, B., He, H., Gao, M., & Gong, D. (2017). Characterizing two types of transient intraseasonal oscillations in the eastern Tibetan Plateau summer rainfall. *Climate Dynamics*, *48*(5–6), 1749–1768. https://doi.org/10.1007/s00382-016-3170-z

Yang, J., Wang, B., Bao, Q., & Bao, Q. (2010). Biweekly and 21-30-day variations of the subtropical summer monsoon rainfall over the lower reach of the Yangtze River Basin. *Journal of Climate*, *23*(5), 1146–1159. https://doi.org/10.1175/2009jcli3005.1

Yang, K., & Wang, C. (2019). Seasonal persistence of soil moisture anomalies related to freeze-thaw over the Tibetan Plateau and prediction signal of summer precipitation in eastern China. *Climate Dynamics*, *53*(3–4), 2411–2424. https://doi.org/10.1007/s00382-019-04867-1

Yang, K., & Zhang, J. (2016). Spatiotemporal characteristics of soil temperature memory in China from observation. *Theoretical and Applied Climatology*, *126*(3–4), 739–749. https://doi.org/10.1007/s00704-015-1613-9

Yang, S., Li, R., Wu, T., Hu, G., Xiao, Y., Du, Y., et al. (2020). Evaluation of reanalysis soil temperature and soil moisture products in permafrost regions on the Qinghai-Tibetan Plateau. *Geoderma*, *377*, 114583. https://doi.org/10.1016/j.geoderma.2020.114583

Ye, D. Z. (1981). Some characteristics of the summer circulation over the Qinghai-Xizang (Tibet) plateau and its neighborhood. *Bulletin of the American Meteorological Society*, *62*(1), 14–19. https://doi.org/10.1175/1520-0477(1981)062<0014:scotsc>2.0.co;2;2

Yeh, T. C., Wetherald, R. T., & Manabe, S. (1984). The effect of soil moisture on the short-term climate and hydrology change–a numerical experiment. *Monthly Weather Review*, *112*(3), 474–490. https://doi.org/10.1175/1520-0493(1984)112<0474:teosmo>2.0.co;2

Zhang, J., Jiang, Y., Chen, H., & Wu, Z. (2018). Double-mode adjustment of Tibetan Plateau heating to the summer circumglobal teleconnection in the Northern Hemisphere. *International Journal of Climatology*, *38*(2), 663–676. https://doi.org/10.1002/joc.5201

Zhang, P., Li, G., Fu, X., Liu, Y., & Li, L. (2014). Clustering of Tibetan Plateau vortices by 10-30-day intraseasonal oscillation. *Monthly Weather Review*, *142*(1), 290–300. https://doi.org/10.1175/mwr-d-13-00137.1

Zheng, Y., Alapaty, K., Herwehe, J. A., Del Genio, A. D., & Niyogi, D. (2016). Improving high-resolution weather forecasts using the weather research and forecasting (WRF) model with an updated Kain-Fritsch scheme. *Monthly Weather Review*, *144*(3), 833–860. https://doi.org/10.1175/mwr-d-15-0005.1

Zhou, Y. S., Deng, G., Gao, S. T., & Xu, X. D. (2002). The wave train characteristics of teleconnection caused by the thermal anomaly of the underlying surface of the Tibetan Plateau. Part I: Data analysis. *Advances in Atmospheric Sciences*, *19*(4), 583–593. https://doi.org/10.1007/s00376-002-0002-3